ARRAY CALIBRATION USING ARRAY RESPONSE INTERPOLATION AND PARAMETRIC MODELING

Bin Yang[a,b], *Tomas McKelvey*[b], *Mats Viberg*[b], *Guanghan Xu*[a]

[a]School of Electronic and Information Engineering, Beihang University, 100191, Beijing, China
[b]Department of Signals and Systems, Chalmers University of Technology, SE-412 96, Gothenburg, Sweden

ABSTRACT

High-performance array applications often require an accurate array response model. A common way to achieve this is by array calibration which involves measuring the response for a finite number of given source directions and employing interpolation. This paper considers the array calibration problem by combing interpolation techniques and parametric modeling. The idea is to model the array response as a product of a mutual coupling matrix, an ideal array response vector (derived from the geometry of antenna array) and an angle-dependent correction vector. Since the major effects are captured by the physical model and the mutual coupling matrix, the correction vector will be a smoother function of angle as compared to direct interpolation of the measured array response. In numerical experiments of a real antenna array, the method is found to improve the performance of the array calibration significantly.

Index Terms—Array calibration, array response interpolation, correction vector, parametric modeling.

1. INTRODUCTION

In antenna array applications it is well known that array modeling errors can have a significant influence on the applications if these effects are not correctly accounted for [1-3]. One remedy to reduce the array modeling errors is array calibration. The calibration methods considered here is based on access to calibration measurements of the real array. A simple method is to use the measured data of the element far-field functions in the array antenna. However to accurately predict the array response at any angles, the grid size must be selected rather small, which would require a large memory storage. Based on the measured array response, an interesting approach is the array interpolation or manifold separation [4-6]. The idea is to use a Fourier representation of the array response in [4], which is based on the manifold separation technique (MST). This requires that the array response has been collected on a uniform grid covering the whole range. In [4], the array interpolation technique is successfully applied in combination with the element-space (ES) root-MUSIC algorithm. However, the method only directly uses the measured array response data, which requires a large number of Fourier terms and hence, more memory to enable an accurate array response. An alternative approach is to use local linear interpolation (LLI) of a factor of the array response model, which is often sufficient [5, 6]. This does not require storing any special parametric data for the array response calibration, such as the Fourier coefficients. The interesting contribution is that an ideal array response vector is decomposed from the array response in these methods. However, these require still a dense grid size to model the array response accurately, since the mutual coupling effects also influence the phase and amplitude of the array response in general.

We are interested in modeling the array response by jointly using the ideal array response (based on the array geometry), an estimated mutual coupling matrix and an angle dependent correction vector based on interpolation where both the mutual coupling matrix and the correction vector is based measurement of the array response. The basic idea is that the correction vector will be much smoother than the true array response, since most of the phase-dependence in one antenna element is due to the mutual coupling and the ideal array response vector. First, a mutual coupling matrix is computed by the simulated (or measured in lab) array response and an isolated element response. The second step is to determine the correction vector at given directions using the measured array response and the estimated mutual coupling matrix. Finally, the array response interpolation is calculated by the interpolation of the correction vector. For a given interpolation grid size, this also results in a more accurate array response model compared to directly interpolate the antenna array measurements.

The original contributions of this paper are the following: a) We show how an exploitation of a simple parametric model of the array response leads to a much smoother interpolation problem than using the original array data; b) We exemplify the idea by applying a simple model of the mutual coupling that can be learned from the measured data. Note that the model need not be perfect for array response interpolation, since the mutual coupling model will be updated by a correction vector.

This paper is organized as follows. In Section 2 we formulate the problem. Next, Section 3 introduces the three calibration methods of the array response including

978-0-9928626-3-3/15/$31.00 ©2015 IEEE

the mutual coupling estimation. A real array of 12 quadrifilar helix antennas (QHAs) is presented in Section 4, whereas Section 5 shows the results of the three calibration methods when applied to the real antenna array. In Section 6, the different approaches are then compared in terms of performance of DOA estimation with MUSIC. The paper is finally concluded in Section 7.

2. PROBLEM FORMULATION

High-performing array applications require that the functional form of the true array response (also called the embedded array response) $\mathbf{a}_{emb}(\eta)$ is accurately known, $\mathbf{a}_{emb}(\eta) = [a_{emb,1}(\eta), \cdots, a_{emb,N}(\eta)]^T$. Here, N is the number of elements in the antenna array located in the x-y plane, and η, which is characterized by the polar angle θ and the azimuth angle ϕ in a 3-dimensional space model, is termed the arrival angle of a signal source.

In an ideal antenna array model, the isolated element pattern is omnidirectional and no mutual coupling exists. Hence, the ideal array response $\mathbf{a}_{ideal}(\eta)$ comes from the geometry only. For a real antenna array, the antenna response of an individual element of the array depends not only on the isolated elements response but also on the presence of all other elements [7]. We assume that the embedded array response has been measured at a grid of angle values, $\eta_1, \eta_2, \cdots, \eta_Q$. With the aid of this calibration data and a simple model of the array response, the goal is to estimate the unknown array response for any angle η.

Assuming that the ideal steering vector $\mathbf{a}_{ideal}(\eta)$ is known, we propose two basic models for the array response.

1) The first model of the embedded array response is

$$\mathbf{a}_{emb}(\eta) = \mathbf{a}_{ideal}(\eta) \odot \mathbf{g}(\eta) \quad (1)$$

where $\odot$ denotes Schur (Hadamard) product and $\mathbf{g}(\eta) = [g_1(\eta), \cdots, g_N(\eta)]^T$ is a correction vector, which is dependent of the angle η. It takes care of the effects of mutual coupling and the properties of the isolated element.

2) The second model is

$$\mathbf{a}_{emb}(\eta) = \mathbf{C}[\mathbf{a}_{ideal}(\eta) \odot \mathbf{g}_e(\eta)] \quad (2)$$

where $\mathbf{C}$ is the $N \times N$ mutual coupling matrix and $\mathbf{g}_e(\eta) = [g_{e,1}(\eta), \cdots, g_{e,N}(\eta)]^T$ is a correction vector, which is also dependent of the angle η. Note that $\mathbf{g}_e(\eta)$ only holds the properties of the isolated element, which is different from the $\mathbf{g}(\eta)$ in the first model case.

Using an accurately measured array response at a given angle, the correction vector $\mathbf{g}(\eta)$ in the first model can be determined as

$$\mathbf{g}(\eta) = \mathbf{a}_{emb}(\eta)./\mathbf{a}_{ideal}(\eta) \quad (3)$$

where $./$ denotes element-wise division.

Given an interpolated $\hat{\mathbf{g}}(\eta)$ at a certain desired angle η, the array response interpolation is then computed as

$$\hat{\mathbf{a}}_{emb}(\eta) = \mathbf{a}_{ideal}(\eta) \odot \hat{\mathbf{g}}(\eta) \quad (4)$$

In addition, if the mutual coupling is known in the second model, the correction vector $\mathbf{g}_e(\eta)$ can be determined at a given angle as

$$\mathbf{g}_e(\eta) = [\mathbf{C}^{-1}\mathbf{a}_{emb}(\eta)]./\mathbf{a}_{ideal}(\eta) \quad (5)$$

Note that if the mutual coupling matrix $\mathbf{C} = \mathbf{I}$, where $\mathbf{I}$ is the identity matrix, the correction vector $\mathbf{g}_e(\eta)$ reduces to $\mathbf{g}_e(\eta) = \mathbf{g}(\eta)$. However, in practice the mutual coupling is typically not an identity matrix. With an interpolated $\hat{\mathbf{g}}_e(\eta)$, the array response interpolation is then computed as

$$\hat{\mathbf{a}}_{emb}(\eta) = \mathbf{C}[\mathbf{a}_{ideal}(\eta) \odot \hat{\mathbf{g}}_e(\eta)] \quad (6)$$

The idea is now that the correction vector $\mathbf{g}(\eta)$ in the first array response decomposition model is smoother than $\mathbf{a}_{emb}(\eta)$ itself, since parts of the phase variation in one embedded element is due to the ideal array response vector $\mathbf{a}_{ideal}(\eta)$. Furthermore, $\mathbf{g}_e(\eta)$ is much smoother than $\mathbf{g}(\eta)$ when $\mathbf{C} \neq \mathbf{I}$, since a part of the phase variation is due to mutual coupling matrix $\mathbf{C}$ and the ideal array response vector $\mathbf{a}_{ideal}(\eta)$. Numerical results of the smoothness, for a real antenna array, are presented in Section 5.

3. LOCAL LINER INTERPOLATION METHODS

3.1. Method 1: The direct interpolation of $\mathbf{a}_{emb}(\eta)$

We consider that the array response is accurately measured at a set of given angles. Here, we will present the local linear interpolation (LLI) of the array response for a 1-D case (azimuth angle ϕ) estimation problem, which is to interpolate the real and imaginary parts of the N elements of the array response to any desired angle [4, 5]. The interpolated response is degraded when the true response is not a smooth function of the angle. In a real antenna array, the important problem is that the function of $\mathbf{a}_{emb}(\phi)$ is difficult to model without any errors.

3.2. Method 2: The interpolation of correction vector $\mathbf{g}(\eta)$

At a fixed θ, the correction vector $\mathbf{g}(\phi)$ can be determined by (3) in the first model using the known array response $\mathbf{a}_{emb}(\phi)$ at a set of given angles. Since the correction vector $\mathbf{g}(\phi)$ is potentially a much smoother function of the angles than $\mathbf{a}_{emb}(\phi)$ is, it is natural to try linear interpolation.

3.3. Method 3: The interpolation of correction vector $\mathbf{g}_e(\eta)$

3.3.1. The mutual coupling matrix is known

Assuming the mutual coupling matrix is known, the correction vector $\mathbf{g}_e(\phi)$ can be determined by (5) in the second model using the known array response $\mathbf{a}_{emb}(\phi)$. The correction vector $\mathbf{g}_e(\phi)$ will be much smoother than the correction vector $\mathbf{g}(\phi)$, provided that $\mathbf{C}$ captures parts of the phase dependence from the mutual coupling. The LLI can also be used to interpolate the real and imaginary parts of $\mathbf{g}_e(\phi)$. Note that, if $\mathbf{C} = \mathbf{I}$, the interpolation Method 3 achieves the same performance as the interpolation Method 2 using LLI.

3.3.2. Estimation of the mutual coupling matrix

In most mutual coupling compensation techniques, a matrix is used to encapsulate the effect of mutual coupling as well as the amplitude and phase distortions caused by imperfect antenna array elements [7, 8]. When the mutual coupling matrix is not known we propose the following strategy. First we assign the correction vector $\mathbf{g}_e(\eta)$ base don the result from measuring each isolated element response in the lab, since $\mathbf{g}_e(\eta)$ only contains the properties of the isolated antenna element. Then, we can estimate mutual coupling $\mathbf{C}$ from the second model.

Assume that there are Q $(Q > N)$ isolated element response data and array response data measured in a lab. From the second model, the optimal mutual coupling matrix $\mathbf{C}$ is then determined using least-squares as

$$\hat{\mathbf{C}} = \arg\min_{\mathbf{C}} \|\mathbf{A}_{emb} - \mathbf{C}\left[\mathbf{A}_{ideal} \odot \mathbf{G}_e\right]\|_F \quad (7)$$

where the subscript F means the Frobenius norm, $\mathbf{A}_{emb} = [\mathbf{a}_{emb}(\eta_1), \cdots, \mathbf{a}_{emb}(\eta_Q)]$ is a matrix of array responses at Q points, $\mathbf{G}_e = [\mathbf{g}_e(\eta_1), \cdots, \mathbf{g}_e(\eta_Q)]$ is a matrix of correction vectors (measured isolated element responses in a lab) at Q points, and $\mathbf{A}_{ideal}$ is a matrix with the corresponding ideal steering vectors.

Normally, the minimum value of the criterion in (7) is not zero when $Q > N$. Hence, we update the estimated correction vector $\tilde{\mathbf{g}}_e(\eta)$ at the given DOAs by

$$\tilde{\mathbf{g}}_e(\eta) = \mathbf{a}_{emb}(\eta)./\left[\hat{\mathbf{C}}\mathbf{a}_{ideal}(\eta)\right] \quad (8)$$

where $\hat{\mathbf{C}}$ is the estimate defined in equation (7). Consequently, the array response interpolation $\hat{\mathbf{a}}_{emb}(\eta)$ can be expressed as

$$\hat{\mathbf{a}}_{emb}(\eta) = \hat{\mathbf{C}}[\mathbf{a}_{ideal}(\eta) \odot \hat{\tilde{\mathbf{g}}}_e(\eta)] \quad (9)$$

where $\hat{\tilde{\mathbf{g}}}_e(\eta)$ is the interpolated estimated correction vector $\tilde{\mathbf{g}}_e(\eta)$.

4. THE REAL ARRAY OF 12 QUADRIFILAR HELIX ANTENNAS

The LEO satellite tests mobile communication technology with a circular array that is composed of $N = 12$ identical quadrifilar helix antennas (QHAs) with respect to rotational symmetry about the origin [9]. The first element is fixed on the x-axis, and the other elements are located clockwise in the x-y plane. The uplink signal wavelength is $\lambda = 150$ mm and the array radius is $r = 150$ mm. Thus, the ideal array response vector can be calculated by

$$\mathbf{a}_{ideal}(\theta,\phi) = \begin{bmatrix} \exp\left(j\frac{2\pi}{\lambda}r\sin\theta\cos\left(\phi - \frac{2\pi\cdot 0}{N}\right)\right) \\ \exp\left(j\frac{2\pi}{\lambda}r\sin\theta\cos\left(\phi - \frac{2\pi\cdot 1}{N}\right)\right) \\ \vdots \\ \exp\left(j\frac{2\pi}{\lambda}r\sin\theta\cos\left(\phi - \frac{2\pi\cdot(N-1)}{N}\right)\right) \end{bmatrix} \quad (10)$$

Instead of measuring the array response of the physical array an accurate electromagnetic simulation can provide the same information. In this paper we use the simulated far-field pattern provided by the CST Microwave Studio software, which is based on the finite integration technique (FIT).

Fig. 1 (a) and (c) represent an isolated antenna element of the QHA it's far-field pattern of amplitude and phase. The isolated element pattern (isolated element response) is due to the properties of the isolated antenna element and is not omnidirectional. Fig. 1 (b) and (d) represent the circular antenna array and the far-field pattern of the first embedded element (the first element of the array response), which is obtained by exciting the first element while all other elements are terminated in their own characteristic impedances. In this antenna array, not only the isolated element patterns are the same (rotated by $2\pi/N$), but also the embedded element patterns are identical due to symmetry:

$$a_{emb,n}(\theta,\phi) = a_{emb,1}\left(\theta, \phi - (n-1)\frac{2\pi}{N}\right) \quad (11)$$

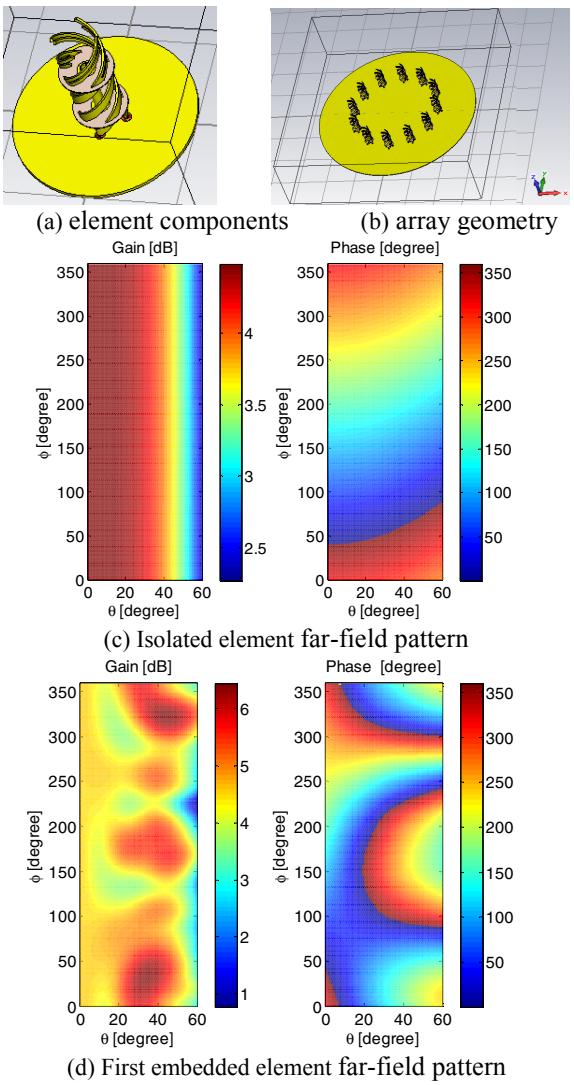

(a) element components (b) array geometry

(c) Isolated element far-field pattern

(d) First embedded element far-field pattern

Fig. 1. Antenna simulation results.

5. CALIBRATION RESULTS

Using data from the QHA array, this section shows the calibration results of the three methods detailed in Section 3. According to symmetry of the antenna array, we just compare the calibration results for one of the elements. Note that our antenna array simulation uses a 1 degree grid size in both θ and ϕ. The precision of interpolation can be described with the average root mean square error (RMSE)

$$RMSE = \sqrt{\frac{1}{I \cdot J} \sum_{i=1}^{I} \sum_{j=1}^{J} \|a(\theta_i, \phi_j) - \hat{a}(\theta_i, \phi_j)\|^2} \quad (20)$$

where I is the total number of test polar angles θ, J is the total number of test azimuth angles ϕ in each θ, $a(\theta_i, \phi_j)$ is the actual value, and $\hat{a}(\theta_i, \phi_j)$ is the estimated value.

The resulting RMSEs of the three interpolation methods of the array response $\mathbf{a}_{emb}(\theta, \phi)$ for one of the elements are shown in Fig. 2. as a function of the interpolation grid size. For an increasing grid size of LLI (i.e. fewer calibration points), the array response estimation error of the three methods is increasing. For a given interpolation grid size $\mid \phi_{l+1} - \phi_l \mid$, it is obvious that Method 3 performs the best, which is to be expected, where $l = 1, 2, \cdots, L-1$, and L is the number of measured calibration points. Also, it is shows that the interpolation errors in Method 3 has the smallest magnitude, since the correction vector $\tilde{\mathbf{g}}_e(\theta, \phi)$ of the Method 3 is much smoother than the correction vector $\mathbf{g}(\theta, \phi)$ of the Method 2, and $\mathbf{g}(\theta, \phi)$ is much smoother than the array response $\mathbf{a}_{emb}(\theta, \phi)$ of the Method 1. The general conclusion is that including the ideal array geometry $\mathbf{a}_{ideal}(\theta, \phi)$ and the mutual coupling matrix leads to that the correction vector $\tilde{\mathbf{g}}_e(\theta, \phi)$ is a smoother function compared to $\mathbf{a}_{emb}(\theta, \phi)$ and hence easier to interpolate with fewer grid points.

6. DOA ESTIMATION WITH MUSIC

Now, we have three models of array response interpolation for DOA estimation. The first model is presented in Section 3.1, which just needs the measured array response

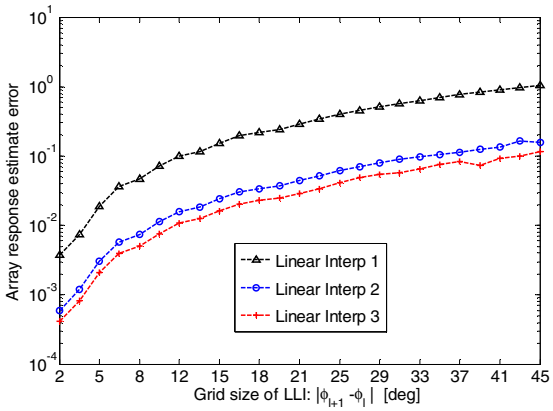

Fig. 2. Computed empirical RMSE by using the three calibration methods versus the grid size.

at given DOAs. The second model is explained in Section 3.2, which needs to know the elements location. The third model is presented in 3.3, which also needs the mutual coupling matrix. Next, we will show some examples of how the different methods affect the DOA estimation with MUSIC on two closely located uncorrelated sources, where the number of snapshots is 100 and the input SNR is 10 dB. A total of 500 trials are conducted for each example. We only show the performance of azimuth angle estimation, since the polar angle estimation presents similar results. The DOA separation $\Delta\phi$ is defined as $\Delta\phi = |\phi_1 - \phi_2|$, where the polar angle is fixed at $45°$. Cases where an algorithm fails to resolve the sources (only one local extremum within $\pm\Delta\phi$ of the true value), or where the DOA estimation error is larger than half the DOA separation, $\Delta\phi$, are declared failures, and these are not included in the RMSE calculation. If the empirical failure rate exceeds 40%, the corresponding RMSE value is not included in the plot.

In the first case, the two sources are fixed at ($\theta_1 = 45°$, $\phi_1 = 100°$) and ($\theta_2 = 45°$, $\phi_2 = 110°$). Figure 3 shows the MUSIC pseudo-spectrum of the DOA estimation using the three interpolation methods for an interpolation grid size of 20 degrees. In Fig. 3, it is clearly seen that the interpolation Method 3 shows the best performance, especially for the location of the pseudo-spectrum peaks. In this scenario, there is only one significant peak in the MUSIC pseudo-spectrum for interpolation Method 1, which directly interpolates the array response, so this method fails to resolve the sources.

In the second case, the azimuth angle ϕ_1 of the first source is fixed at $100°$ and the second varied between $\phi_2 = 103°$ and $\phi_2 = 160°$. Here, we use 21 degrees grid size in the three interpolation methods. The performance

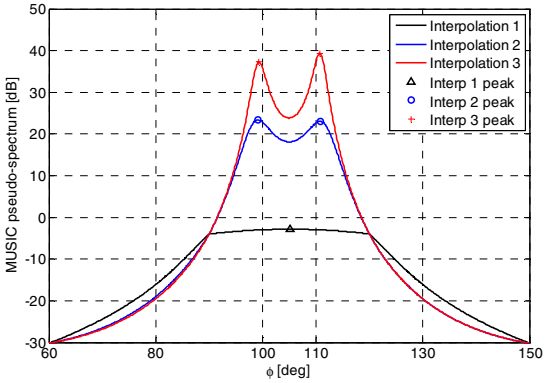

Fig. 3. MUSIC pseudo-spectrum for 20 degrees interpolation grid size

of MUSIC with the empirical resulting RMSE of the three interpolation methods is plotted in Fig. 4. It is clearly seen that the three methods ameliorate significantly with increasing DOA separation $\Delta\phi$, and interpolation Method 3 again shows the best performance for a given source separation. It is interesting to note that Method 1 fails, when the source separation is smaller than 9 degrees separation. However, Method 2 and Method 3 break down at 7 degrees and 5 degrees source separation, respectively, since the correction vectors $\mathbf{g}(\theta, \phi)$ and $\tilde{\mathbf{g}}_e(\theta, \phi)$ are smoother than $\mathbf{a}_{emb}(\theta, \phi)$. This clearly shows that the third interpolation method not only improves the DOA estimation accuracy, but also can be used in scenarios with smaller source separation.

In the third case, the source separation $\Delta\phi$ is fixed at $6°$, the azimuth angle ϕ_1 of the first source is varied from $\phi_1 = 30°$ to $\phi_1 = 150°$. Fig. 5 displays measured performance of the three interpolation methods with MUSIC versus the grid size. The three methods deteriorate significantly with increasing the grid size. For a given grid size of LLI, it is clearly seen that Method 1 performs the worst

among the interpolation techniques in this scenario. We also note that Method 1 will fail, when the grid size of LLI is larger than the source separation ($\Delta\phi = 6°$). In contrast, when we include models of the ideal array response and mutual coupling as in Method 2 and Method 3, a larger grid size of LLI can be used. Method 2 breaks down at 20 degrees grid size and Method 3 breaks down at 33 degrees grid size. It is clear that the interpolation grid size can be more sparse using Method 3 for a given performance requirement.

7. CONCLUSION

This paper presents a new method for array calibration combining a model of the ideal response, a mutual coupling matrix and a correction vector based on linear interpolation. This method combines interpolation techniques with parametric modeling. Since parts of the phase variation in one embedded element of the array response is due to the mutual coupling and the ideal array steering vector, interpolation of the correction vector yields a much more accurate model for each element separately, which is then used to update the array response.

The method is tested using a real antenna array and it is shown to improve the calibration performance significantly. We can easily apply the interpolation of the correction vector with an estimated mutual coupling matrix and a measured array response for array calibration. The results also show that the method with correction vector interpolation and mutual coupling estimation outperforms the direct interpolation method that only uses the measured array response for a given grid. The improved array response interpolation is also shown to lead to improved DOA estimation performance for a given interpolation grid size.

REFERENCES

[1] J. Dai and W. Xu, "Real-valued DOA estimation for uniform linear array with unknown mutual coupling," *Signal Processing*, vol. 92, pp.2056-2065, 2012.

[2] Y. Yu, H. S. Lui, C. H. Niow and H. T. Hui, "Improved DOA estimations using the receiving mutual impedances for mutual coupling compensation: an experimental stury", *IEEE Trans. Signal Processing*, vol. 10, no. 7, pp. 2228-2233, Jul. 2011.

[3] P. Heidenreich, A. M. Zoubir and M. Rubsamen, "Joint 2-D DOA estimation and phase calibration for uniform rectangular arrays," *IEEE Trans. Signal processing*, vol. 60, no. 9, pp. 4683-4693, Sep. 2012

[4] F. Belloni, A. Richter and V. Koivunen, "DoA estimation via manifold separation for arbitrary array structures," *IEEE Trans. Signal Processing*, vol. 55, no. 10, Oct. 2007, pp.4800-4810.

[5] M. Lanne, A. Lundgren and M. Viberg, "Calibrating an array with scan dependent errors using a sparse grid," in *Conf. Rec. 2006 Fortieth Asilomar Conf. Signals, Systems and Computers*, Pacific Grove, CA, USA, Oct, 2006, pp. 2242-2246.

[6] M. Viberg and A. Lundgren, "Array interpolation based on local polynomial approximation with application to DOA estimation using weighted MUSIC," in *Conf. Rec. 2009 IEEE Int. Conf. Acoustics, Speech and Signal Processing*, Taipei, Apr, 2009, pp. 2145-2148.

[7] Q. L. Huang, H. X. Zhou, J. H. Bao and X. W. Shi, "Mutual coupling calibration for microstrip antenna arrays via element pattern reconstruction method," *IEEE Antennas and Wireless Propagation Letters*, vol. 13, pp. 51–54, 2014.

[8] J. F. Izquierdo, J. Rubio and J. Zapata, "A fast technique to estimate the mutual coupling coefficients from the transmitting characteristics of an isolated element," *IEEE Antennas and Wireless Propagation Letters*, vol. 9, pp. 1182–1185, 2010.

[9] B. Yang, F. He, J. Jin, H. G. Xiong and G. H. Xu, "DOA estimation for attitude determination on communication satellites," *Chinese Journal of Aeronautics*, vol. 27, no. 3, pp. 670–677, 2014.

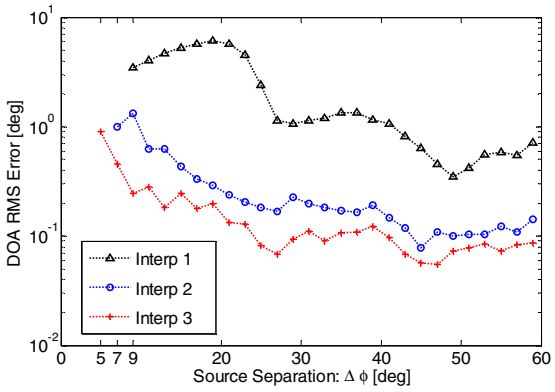

Fig. 4. DOA RMS Error performance of the three interpolation methods versus the source separation.

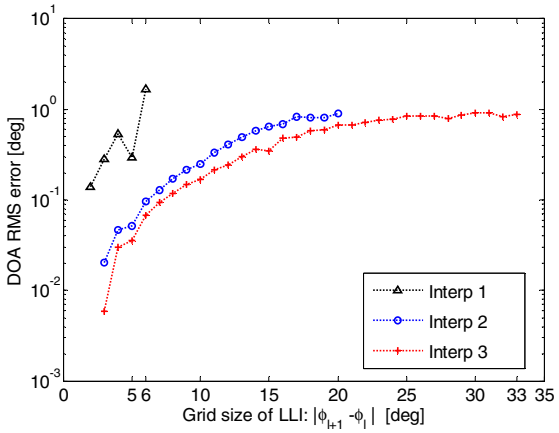

Fig. 5. DOA RMS Error performance of the three interpolation methods versus the grid size.